Research Article | Vol. 25, No. 4 | 20 Feb 2017 | OPTICS EXPRESS 3709

Optics EXPRESS

Improving cavity-enhanced spectroscopy of molecular ions in the mid-infrared with up-conversion detection and Brewster-plate spoilers

CHARLES R. MARKUS,[1] ADAM J. PERRY,[1] JAMES N. HODGES,[2] AND BENJAMIN J. MCCALL[1,3,*]

[1]*Department of Chemistry, University of Illinois at Urbana-Champaign, Urbana, IL, 61801, USA*
[2]*Current address: Department of Chemistry, Old Dominion University, Norfolk, VA 23529, USA*
[3]*Departments of Astronomy and Physics, University of Illinois at Urbana-Champaign, Urbana, IL, 61801, USA*
[*]*bjmccall@illinois.edu*
http://bjm.scs.illinois.edu/

Abstract: The performance of sensitive spectroscopic methods in the mid-IR is often limited by fringing due to parasitic etalons and the background noise in mid-infrared detectors. In particular, the technique Noise Immune Cavity Enhanced Optical Heterodyne Velocity Modulation Spectroscopy (NICE-OHVMS), which is capable of determining the frequencies of strong rovibrational transitions of molecular ions with sub-MHz uncertainty, needs improved sensitivity in order to probe weaker transitions. In this work, we have implemented up-conversion detection with NICE-OHVMS in the 3.2 – 3.9 μm region to enable the use of faster and more sensitive detectors which cover visible wavelengths. The higher bandwidth enabled detection at optimized heterodyne frequencies, which increased the overall signal from the H_3^+ cation by a factor of three and was able to resolve sub-Doppler features which had previously overlapped. Also, we demonstrate the effectiveness of Brewster-plate spoilers to remove fringes due to parasitic etalons in a cavity enhanced technique. Together, these improvements reduced the instrument's noise equivalent absorption to 5.9×10^{-11} cm^{-1} Hz$^{-1/2}$, which represents a factor of 34 improvement in sensitivity compared to previous implementations of NICE-OHVMS. This work will enable extended high-precision spectroscopic surveys of H_3^+ and other important molecular ions.

OCIS codes: (190.7220) Upconversion; (300.6310) Spectroscopy, heterodyne; (300.6340) Spectroscopy, infrared; (300.6380) Spectroscopy, modulation; (300.6390) Spectroscopy, molecular; (300.6460) Spectroscopy, saturation.

References and links

1. T. P. Snow and V. N. Bierbaum, "Ion chemistry in the interstellar medium," Annu. Rev. Anal. Chem. **1**, 229–259 (2008).
2. L. Lodi, O. L. Polyansky, J. Tennyson, A. Alijah, and N. F. Zobov, "QED corrections for H_3^+," Phys. Rev. A. **89**(3), 032505 (2014).
3. H. -C. Chen, C. -Y. Hsiao, J. -L. Peng, T. Amano, and J. -T. Shy, "High-resolution sub-Doppler Lamb dips of the ν_2 fundamental band of H_3^+," Phys. Rev. Lett. **109**(26) 263002 (2012).
4. O. Asvany, J. Krieg, and S. Schlemmer, "Frequency comb assisted mid-infrared spectroscopy of cold molecular ions," Rev. Sci. Instrum. **83**(9) 093110 (2012).
5. J. N. Hodges, A. J. Perry, P. A. Jenkins II, B. M. Siller, and B. J. McCall, , "High-precision high-accuracy rovibrational spectroscopy of molecular ions," J. Chem. Phys. **139**(16), 164201 (2013).
6. J. Ye, L.-S. Ma, and J. L. Hall, "Ultrasensitive detections in atomic and molecular physics: demonstration in molecular overtone spectroscopy," J. Opt. Soc. Am. B **15**(1) 6–15 (1998).
7. C. S. Gudeman, M. H. Begemann, J. Pfaff, and R. J. Saykally, "Velocity-modulated infrared laser spectroscopy of molecular ions: the ν_1 band of HNN^+," J. Chem. Phys. **78**(9) 5837–5838 (1983).
8. A. J. Perry, J. N. Hodges, C. R. Markus, G. S. Kocheril, and B. J. McCall, "Communication: High precision sub-Doppler infrared spectroscopy of the HeH^+ ion," J. Chem. Phys. **141**(10), 101101 (2014).
9. A. J. Perry, J. N. Hodges, C. R. Markus, G. S. Kocheril, and B. J. McCall, "High-precision, *R*-branch transition frequencies in the ν_2 fundamental band of H_3^+," J. Mol. Spectrosc. **317**(10), 71–73 (2015).

#281870 https://doi.org/10.1364/OE.25.003709
Journal © 2017 Received 5 Dec 2016; revised 25 Jan 2017; accepted 27 Jan 2017; published 10 Feb 2017

Optics EXPRESS

10. C. R. Markus, J. N. Hodges, A. J. Perry, G. S. Kocheril, H. S. P. Müller, and B. J. McCall, "High precision rovibrational spectroscopy of OH^+," Astrophys. J. **817**(2), 138 (2016).
11. C. Langrock, E. Diamanti, R. V. Roussev, Y. Yamamoto, and M. M. Fejer, "Highly efficient single-photon detection at communication wavelengths by use of upconversion in reverse-proton-exchanged periodically poled $LiNbO_3$ waveguides," Opt. Lett. **30**(13) 1725–1727 (2005).
12. M. J. Khan, J. C. Chen, and S. Kaushik, "Optical detection of terahertz radiation by using nonlinear parametric upconversion," Opt. Lett. **32**(22), 3248–3250 (2007).
13. K. Karstad, A. Stefanov, M. Wegmuller, H. Zbinden, N. Gisin, T. Aellen, M. Beck, and J. Faist, "Detection of mid-IR radiation by sum frequency generation for free space optical communication," Opt. Laser Eng. **43**, 537–544 (2005).
14. P. Ehlers, A. C. Johansson, I. Silander, A. Foltynowicz, and O. Axner, "Use of etalon-immune distances to reduce the influence of background signals in frequency-modulation spectroscopy and noise-immune cavity-enhanced optical heterodyne molecular spectroscopy," J. Opt. Soc. Am. B **31**(12), 2938–2945 (2014).
15. E. A. Whittaker, M. Gehrtz, and G. C. Bjorklund, "Residual amplitude modulation in laser electro-optic phase modulation," J. Opt. Soc. Am. B **2**(8) 1320–1326 (1985).
16. C. R. Webster, "Brewster-plate spoiler: a novel method for reducing the amplitude of interference fringes that limit tunable-laser absorption sensitivities," J. Opt. Soc. Am. B **2**(9), 1464–1470 (1985).
17. K. N. Crabtree, J. N. Hodges, B. M. Siller, A. J. Perry, J. E. Kelly, P. A. Jenkins II, B. J. McCall, "Sub-Doppler mid-infrared spectroscopy of molecular ions," Chem. Phys. Lett. **551**, 1–6 (2012).
18. R. W. P. Drever, J. L. Hall, F. V. Kowalski, J. Hough, G. M. Ford, A. J. Munley, and H. Ward, "Laser phase and frequency stabilization using an optical resonator," Appl. Phys. B-Photo. **31**(2) 97–105 (1983).
19. B. M. Siller, A. A. Mills, and B. J. McCall, "Cavity-enhanced velocity modulation spectroscopy," Opt. Lett. **35**(8), 1266–1268 (2010).
20. O. Axner, W. Ma, and A. Foltynowicz, "Sub-Doppler dispersion and noise-immune cavity-enhanced optical heterodyne molecular spectroscopy revised," J. Opt. Soc. Am. B **25**(7) 1166–1177 (2008).
21. G. D. Boyd and D. A. Kleinman, "Parametric interaction of focused Gaussian light beams," J. Appl. Phys. **39**(8), 3597–3639 (1968).
22. A. V. Smith, "SNLO nonlinear optics code," AS-Photonics, Albuquerque, NM, http:/www.as-photonics.com/SNLO.htmls
23. P. Werle, R. Mücke, and F. Slemr, "The limits of signal averaging in atmospheric trace-gas monitoring by tunable diode-laser absorption spectroscopy (TDLAS)," Appl. Phys. B-Photo **57**(2) 131–139 (1993).
24. R. G. DeVoe and R. G. Brewer, "Laser-frequency division and stabilization," Phys. Rev. A **30**(5), 2827–2829 (1984).

1. Introduction

Accurate and precise measurements of rovibrational transitions of molecular ions have led to discoveries of important processes in the interstellar medium and have provided valuable benchmarks for cutting-edge potential energy surfaces from *ab initio* theory [1, 2]. In the past five years, new laboratory techniques have been developed that can determine rovibrational transitions of molecular ions with sub-MHz precision [3–5]. One such technique is Noise Immune Cavity Enhanced Optical Heterodyne Velocity Modulation Spectroscopy (NICE-OHVMS), which combines the sensitivity of Noise-Immune Cavity-Enhanced Optical Heterodyne Molecular Spectroscopy (NICE-OHMS) [6] with the ion-neutral discrimination of velocity modulation spectroscopy (VMS) [7].

Instead of directly measuring absorption, NICE-OHMS measures the difference in absorption and dispersion at the different components of a frequency modulation (FM) triplet, which is composed of a central carrier and two sidebands spaced by the modulation frequency. If the modulation frequency is set to an integer multiple of a cavity's free spectral range (FSR), the entire triplet can be resonantly coupled into the cavity yielding a significant boost in signal. An additional benefit is the "noise immunity", which is the ability to reduce noise from a poor laser-to-cavity lock– if the laser is slightly off resonance, all three components of the FM triplet are affected identically. By adding VMS detection, we can discriminate signals from ions and neutrals while gaining an additional layer of modulation. Within an AC discharge, ions will follow the electric field which results in an oscillating Doppler profile, and the modulated signal can be recovered by a lock-in amplifier.

With NICE-OHVMS, we have successfully measured a number of transitions of H_3^+, HeH^+, and OH^+ with the highest precision to date [5,8–10]. However, insufficient signal-to-noise (S/N)

Optics EXPRESS

of many transitions has limited the extent of these studies, and only the frequencies of the strongest transitions within the fundamental bands were determined with sub-MHz precision. The insufficient S/N can be attributed to the lack of sensitive detectors in the mid-infrared (mid-IR) and the presence of parasitic etalons.

Mid-IR transitions are far from the coverage of detectors with the best noise characteristics in the near-IR and visible. Although many overtone transitions are in the near-IR, corresponding transitions within fundamental bands in the mid-IR are at least an order of magnitude stronger. Up-conversion detection is capable of overcoming this limitation by enabling the measurement of mid-IR transitions with near-IR and visible detectors using difference or sum frequency generation (DFG or SFG). The mid-IR light is converted to wavelengths within the coverage of silicon detectors while maintaining the frequency and velocity modulation signals. Up-conversion has enabled mid-IR single-photon counting experiments, sensitive THz detection at room temperature, and has improved wireless communication with quantum cascade lasers [11–13]. In this work, up-conversion through DFG has been implemented into the NICE-OHVMS technique, which has enabled the use of a faster and more sensitive silicon detector. However, the benefits from up-conversion could not be realized until periodic signals from etalons were removed from the background.

Parasitic etalons have long plagued sensitive spectroscopic techniques. The interference from light reflecting between parallel surfaces can easily obscure weak signals. Other frequency modulation spectroscopy (FMS) techniques have fought this by separating optics at etalon-immune distances [14, 15]. The strength of the fringes from an etalon in an FMS experiment is different for absorption and dispersion and depends on the ratio between modulation frequency (ν_m) and the FSR of the etalon. Fringes appearing in dispersion have a $\sin(2\pi\nu_m/\mathrm{FSR})$ dependence, whereas those in absorption take the form of $\sin^2(2\pi\nu_m/\mathrm{FSR})$ [14]. Etalon immune distances work by setting the modulation frequency to be an integer multiple of the FSR of the etalon, which removes the signal in absorption and dispersion. However, experimental constraints can necessitate low modulation frequencies making the etalon-immune distance impractically long. Another solution is to rapidly change the positions of the interference fringes and average them out [16]. In the past, this has been avoided by NICE-OHMS and other cavity enhanced techniques because it was thought that it could disrupt the lock to the cavity. We have found that a rapidly rotated CaF_2 window set in our optical path is capable of removing fringes from NICE-OHVMS scans without introducing other forms of noise. This has nearly eliminated the signals from parasitic etalons in our instrument.

Optics EXPRESS

2. Experimental

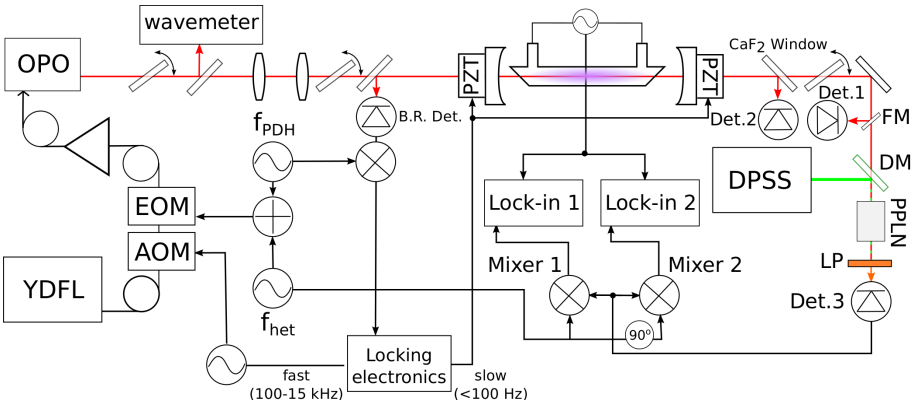

Fig. 1. Experimental layout. YDFL: ytterbium doped fiber laser, AOM: acousto-optic modulator, EOM: electro-optic modulator, OPO: optical parametric oscillator, PZT: piezoelectric transducer, DPSS: diode-pumped solid-state laser, f_{het}: Heterodyne frequency, f_{PDH}: Pound-Drever-Hall frequency, Det. 1: mid-IR transmission detector (Vigo PVM-10.6), B.R. Det.: back reflection detector (Boston Electronics Vigo PVI-4TE-6), Det. 2: mid-IR transmission detector (Boston Electronics Vigo PVI–4TE-6), Det. 3: silicon detector (Thorlabs DET025A), FM: flipper mirror, DM: dichroic mirror, PPLN: periodically poled lithium niobate crystal, and LP: longpass filter.

A block diagram of the instrument is shown in Fig. 1. The technique builds upon the NICE-OHVMS instrument which has been described in previous publications [5,17]. In brief, 1064 nm light from a ytterbium-doped fiber laser is first sent to a fiber-coupled acousto-optic modulator (AOM) for frequency corrections and then phase modulated by a fiber-coupled electro-optic modulator (EOM) to produce two sets of sidebands for Pound-Drever-Hall (PDH) locking [18] and heterodyne detection. The output from the EOM is amplified by an erbium doped fiber amplifier and fed into an optical parametric oscillator (OPO) which produces an idler (1 W, 3.2 - 3.9 μm) and a signal beam through parametric down-conversion. The idler beam is coupled into an external cavity (finesse 100) which contains a positive column discharge cell. The heterodyne frequency is set to an integer multiple of the FSR, allowing the sidebands and carrier to be resonant with the cavity. H_3^+ ions are produced by flowing 300 mTorr of hydrogen in a glow discharge cell while liquid nitrogen was flowed around the jacket surrounding the inner bore. The electrodes were driven sinusoidally at 40 kHz by a step-up transformer.

Light reflected off the cavity was picked off with a CaF_2 window and focused onto a thermoelectrically cooled fast mid-IR detector (Boston Electronics Vigo PVI-4TE-6) and used to produce the PDH error signal. This was sent to the locking electronics which produce slow corrections (<100 Hz) which are sent to two piezoelectric transducers which control the cavity length. The fast corrections (100 Hz - 15 kHz) are sent to the AOM.

A fraction of the light transmitted from the cavity was picked off with a CaF_2 window and further attenuated with a wire-grid polarizer. The light was focused onto another thermoelectrically cooled fast mid-IR detector (Det. 2, Boston Electronics Vigo PVI-4TE-6), which has a 3 dB bandwidth (BW) of 600 MHz and a noise equivalent power (NEP) of 1.67×10^{-12} W Hz$^{-1/2}$. The light transmitted through the window was either sent to a slower mid-IR detector (Det. 1, Boston Electronics Vigo PVM-10.6) with a 3 dB BW of 160 MHz and NEP of 4.76×10^{-9} W Hz$^{-1/2}$, which was used in previous iteration of the instrument, or to the DFG optics. For DFG, the transmitted idler was colinearized with a high power (6.4 W) 532

Optics EXPRESS

nm beam from a diode-pumped solid-state laser (Coherent V10) using a dichroic mirror (ISP Optics) and focused into a 4 cm MgO doped periodically poled lithium niobate (PPLN) crystal (MSFG612, Covesion Ltd). The optics before the dichroic mirror were designed to produce a confocal range (twice the Rayleigh range) equal to the length of the PPLN crystal. The PPLN crystal has poling periods from 10.4 - 11 μm and its temperature can be set from 30 - 200 °C, covering 3.2 - 3.9 μm. The up-converted light (616 - 638 nm) was selected with a long-pass filter and focused onto a fast silicon biased detector (Det. 3,Thorlabs DET025A) with a 3 dB BW of 2 GHz and NEP of 9.29 $\times 10^{-15}$ W Hz$^{-1/2}$.

Brewster-plate spoilers [16] were used to average out parasitic etalons in the system. This was accomplished by mounting CaF_2 windows onto galvanometers which were driven by a 35 Hz sawtooth wave for a full sweep of 1°. These were placed after the OPO, the mode-matching telescope, and the output mirror of the cavity.

For any given scan, the transmitted light was detected with Det. 1, 2, or 3. The output was first demodulated by a pair of electronic mixers referenced to the heterodyne frequency and set 90° out of phase with one another. The output of each mixer was then sent to a separate two-channel lock-in amplifier referenced to twice the frequency driving the plasma to recover the velocity modulated signal [19]. Each lock-in amplifier produces the in-phase and quadrature components with respect to velocity modulation, resulting in two channels of detection for each mixer. All spectra were of the $R(1,0)$ transition of H_3^+ at 2725.8984 cm^{-1}. Scans were collected with the heterodyne modulation frequency set to 1, 3, and 5×FSR of the cavity (77, 231, and 385 MHz). Each scan shown is a result of stepping the laser in 3 MHz increments over the entire scan window and recording each data point with a 300 ms time constant.

3. Results & discussion

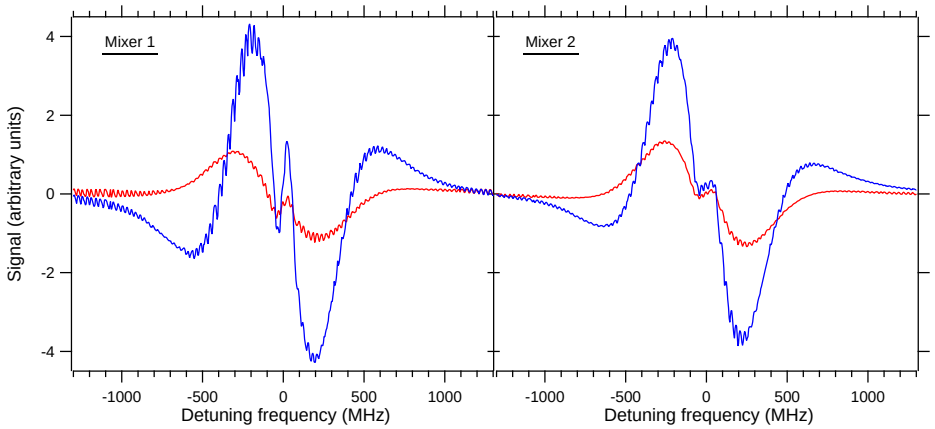

Fig. 2. A NICE-OHVMS scan of the $R(1,0)$ transition of H_3^+, centered at 81720377 MHz (2725.8984 cm^{-1}) with the heterodyne frequency set to 1×FSR of the cavity (77.304 MHz). The in-phase (red) and quadrature (blue) components of the velocity modulation signal are plotted for both the in-phase (left) and quadrature (right) components of the heterodyne signal. This scan was recorded with Det. 1.

An example of a NICE-OHVMS scan using the original detector (Det. 1) and without the Brewster-plate spoilers can be seen in Fig. 2. The two layers of modulation produce the overall odd lineshape. The phase-modulated light produces an FM triplet composed of a carrier and two sidebands separated by the modulation frequency. Each sideband produces a beat note with

Optics EXPRESS

the carrier, which effectively cancel each other out when the triplet is balanced. If one or more components are on resonance with a transition, it disrupts the balance of the triplet and produces an intensity modulation of the light at the heterodyne frequency. The signal's strength and phase depend on the difference in absorption and dispersion of the sidebands and the carrier.

The second layer of modulation is velocity modulation. Within the discharge, the ions will follow the electric field causing their velocity distribution to oscillate at the frequency driving the plasma. In a single pass experiment, the signal from a charged carrier can be recovered with a lock-in amplifier referenced to the discharge frequency. In our case, the bidirectional nature of the cavity causes a simultaneous blue and red shift, and the signal is instead modulated at twice the driving frequency. The ions are also created and destroyed at twice the driving frequency, causing additional concentration modulation. Both the velocity and concentration modulation signals are recovered by the lock-in amplifiers. A more in depth description of cavity enhanced velocity modulation can be found in Siller *et. al* [19].

The sub-Doppler features at the center of the transition are the result of the high intracavity power and the bidirectional cavity. There are two counter propagating FM triplets, and each component can act as a pump/probe. When two counter propagating beams interact with the same velocity component, a Lamb dip can be formed that is much narrower than the overall profile. As the FM triplet is scanned over a transition, Lamb dips will occur at half-integer multiples of the heterodyne frequency centered around the rest frequency of the transition [20]. In Fig. 2, the output from mixer 1 shows a central dispersion Lamb dip, while mixer 2 shows the first order absorption Lamb dips. A least-squares fitting routine can be used to determine the line centers with sub-MHz precision, as described in depth by Crabtree *et. al* [17].

3.1. Brewster-plate spoiler

Initially, our system had a number of etalons which spanned from 50 cm to 5 m in length, the effects of which can be seen in Fig. 2 as fringing. For an etalon to be detectable, it must persist through demodulation at both the heterodyne frequency and twice the frequency driving the electrodes. An etalon can disrupt the balance of the FM triplet producing residual amplitude modulation (RAM), resulting in fringes spaced by the FSR in both absorption and dispersion [14]. While one might naively think that demodulating at the velocity modulation frequency would reject the RAM produced by an etalon, this is clearly not the case. One possible mechanism which would further affect the FM triplet at the velocity modulation frequency could be the changing index of refraction within the optical cavity. Because the refractive index will change with the concentration of ions and neutrals within the plasma, it will cycle twice every discharge period. This would cause the longitudinal modes of the cavity to modulate and, if the PDH correction bandwidth is too slow, would introduce an intensity modulation at twice the driving frequency of the discharge. This would allow for the RAM of the etalon to pass through both layers of modulation.

Regardless of the mechanism, fringes from etalons do appear in the baseline of NICE-OHVMS scans and it should be possible to eliminate them with conventional methods. If the two surfaces of an unwanted etalon are separated such that ν_{het} = FSR the signal would go to zero since all three components of the FM triplet are affected equally. Previously, the modulation frequency in our experiment was limited to 77 MHz by the bandwidth of the detector making the required etalon immune distance 1.9 m, which would be impractical. The large detection bandwidth of Det. 2 and Det. 3 make it possible to increase the heterodyne frequency and reduce the etalon immune distance. Instead, a more flexible approach was taken.

Webster demonstrated that interference fringes could be averaged out by placing a Brewster-plate spoiler within the etalon [16]. A Brewster-plate spoiler is a window mounted at Brewster's angle on a galvanometer that is driven by a triangular wave, which rapidly changes the optical path length of the etalon. The change in optical path length (OPL) caused by placing a window

Optics EXPRESS

within an etalon is shown in Fig. 3. Rotating the window causes the frequency of individual fringes to shift rapidly. The change in path-length when the window is rotated from angle θ_{i1} to θ_{i2} was derived by Webster and is expressed by the following:

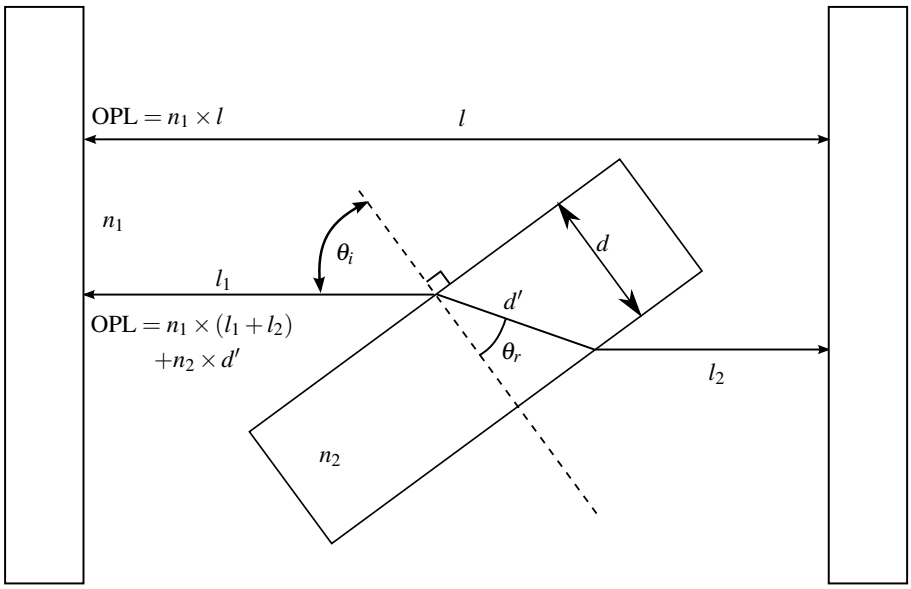

Fig. 3. A depiction of the change in optical path length (OPL) to an etalon of length l when a window with a refractive index n_2, thickness d, and incident angle θ_i is placed between the reflective surfaces.

$$\Delta\text{OPL} = d_1'[\cos(\theta_{i1} - \theta_{r1}) + n_2] - d_2'[\cos(\theta_{i2} - \theta_{r2}) + n_2] \tag{1}$$

where ΔOPL is the change in the optical path length, θ_{i1} and θ_{i2} are the incident angles, θ_{r1} and θ_{r2} are the refracted angles, $d_i' = d/\cos(\theta_{ri})$ for the window's thickness d, and n_2 is the index of refraction of the plate. With a wavelength of 3.668 μm, a CaF_2 window with a thickness of 5 mm, a refractive index of 1.41, and the window placed at Brewster's angle (54.7°) for maximum transmission, a change of 1° leads to a change in optical path length of 72 μm. The shift in frequency which will occur from this is:

$$\Delta\nu = \frac{\nu\Delta\text{OPL}}{\text{OPL}} \tag{2}$$

The number of fringes for each sweep can be found by dividing by the etalon's FSR, yielding:

$$\frac{\Delta\nu}{\text{FSR}} = \frac{2\nu\Delta\text{OPL}}{c} = \frac{2\Delta\text{OPL}}{\lambda} \tag{3}$$

where λ is the vacuum wavelength. Therefore, a shift of 1° will average over 40 fringes in a single sweep and is independent of the etalon's length. We found that it took three total Brewster-plate spoilers to remove all observable etalon fringes; these were placed directly after the OPO, between the mode-matching telescope and the first cavity mirror, and in between the second cavity mirror and the detector. The effect can be seen in Figs. 4 and 5. In Fig. 5, the signal to noise increased from 125 to 2000 in the best channel.

An initial concern was the offset in the position of the laser beam that occurs as the angle of the window changes, which could disrupt the PDH lock to the cavity. However, despite two

Optics EXPRESS

Brewster-plate spoilers being placed between the cavity and the OPO it did not introduce any significant noise to the scan.

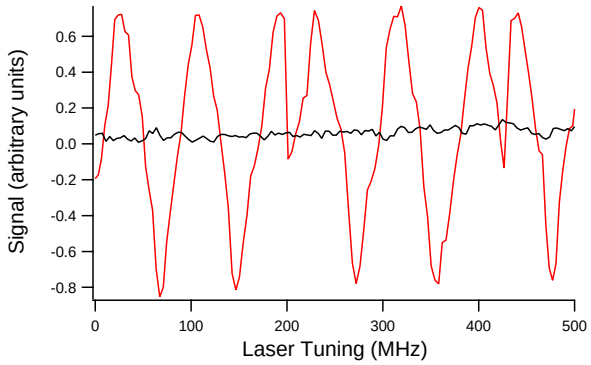

Fig. 4. Comparison between the baseline when the galvanometer is on (black trace) or off (red trace). The discontinuities in the fringe every ~200 MHz are caused when the cavity is relocked, which changes the optical path length of the etalon.

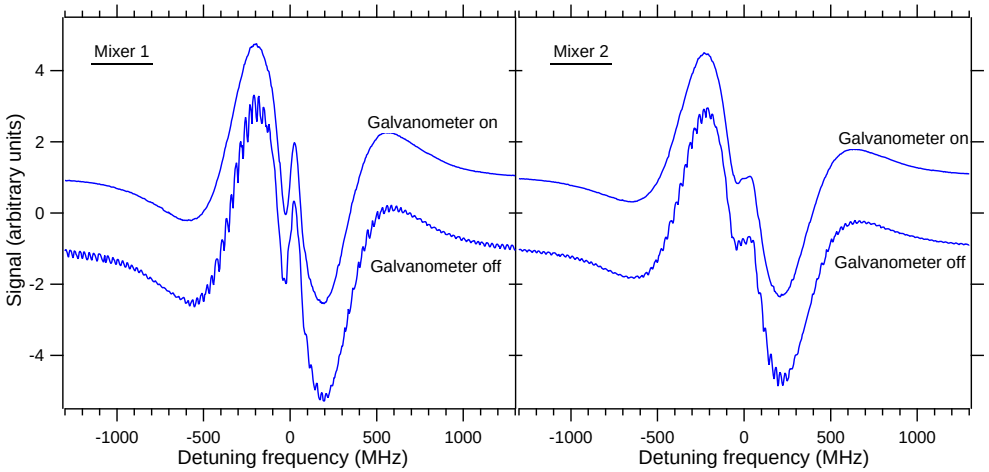

Fig. 5. Comparison between two scans of the H_3^+ $R(1,0)$ transition with the galvanometer on (top) and galvanometer off (bottom). All traces are of the quadrature component of the lock-in amplifiers. Offsets were added for clarity.

3.2. *Up-conversion detection*

Difference frequency generation is a nonlinear process which takes two pump beams at frequencies ν_1 and ν_2 where $\nu_1 > \nu_2$, to produce a third ν_3 which follows the conservation of energy $\nu_1 - \nu_2 = \nu_3$. As a coherent process, the phase matching between the three beams is vital for effective conversion, *i.e.* $\Delta\boldsymbol{k} = \boldsymbol{k_1} - \boldsymbol{k_2} - \boldsymbol{k_3} = 0$, where $\boldsymbol{k_i}$ are the wave vectors. Angle phase matching in birefringent crystals was the original method for meeting this criterion. Modern optics make use of quasi-phase matching, where the crystals are grown to have the crystal orientation periodically changed over length Λ, which changes the phase matching requirement

Optics EXPRESS

to $\Delta \boldsymbol{k} = \pi/\Lambda$. The intensity and interaction time determine the efficiency of the conversion. The Boyd-Kleinman focusing condition states that the maximum conversion efficiency occurs when the confocal length (twice the Rayleigh range) is equal to the length of the crystal [21]. With a 4 cm PPLN crystal, we generated 3 mW of 622 nm light from 70 mW of 3.667 μm light transmitted from the cavity and 6.4 W of 532 nm light. This equates to a conversion efficiency $\eta_{DFG} = (P_{DFG}/P_{mid-IR})/P_{pump} = 6.7 \times 10^{-3}$/W, where P_{pump} is the power of the 532 nm beam. The theoretical conversion efficiency was calculated with the SNLO software package [22] to be 1.2×10^{-2}/W. The discrepancy between the theoretical and measured efficiency is likley due to reflections off the PPLN input surface, absorption within PPLN, imperfect beam overlap, and a suboptimal confocal range.

The conversion efficiency was more than adequate when considering the sensitivity of the silicon detector. Up-conversion detection will ultimately sacrifice power for speed and sensitivity. Detector sensitivity is usually reported in noise equivalent power (NEP) in units of W/Hz$^{1/2}$, which represents the amount of power required to produce a response with a S/N of 1 with a 1 Hz bandwidth. To compare all three detectors, it is important to consider how each is implemented into the NICE-OHMVS instrument, where the NEP should be converted to the noise equivalence of power transmitted from the cavity. To determine how much mid-IR power is required to produce a S/N of 1 with a bandwidth of 1 Hz, the NEP of the detector must be divided by the fraction of mid-IR power converted by DFG, which is calculated with $\eta_{DFG} \times P_{pump}$. The total expression for NEP$_{eff}$ is shown in Eq. 4.

$$\text{NEP}_{eff} = \text{NEP}_{Det.3}/(\eta_{DFG} \times P_{pump}) \tag{4}$$

Here, NEP$_{eff}$ is the effective noise equivalent power of the detector, NEP$_{Det.3}$ is the noise equivalent power of Det. 3, and η_{DFG} is the efficiency of the DFG process in units of W^{-1}. For Det. 2, the losses from taking only a fraction of the light must be considered which is calculated by Eq. 5.

$$\text{NEP}_{eff} = \text{NEP}_{Det.2}/(P_{inc}/P_{tot}) \tag{5}$$

Here, NEP$_{Det.2}$ is the noise equivalent power of Det. 2, P_{inc} is the power incident on the detector, and P_{tot} is the total power transmitted from the cavity. This conversion was unnecessary for Det. 3 since all light produced by DFG was focused onto the detector. Using NEP$_{eff}$ allows for a direct comparison between the sensitivity of the three detection schemes, as shown in Table 1. The comparison shows that, despite the suboptimal conversion efficiency, up-conversion should still have improved noise characteristics. Baseline measurements were collected for each detection scheme in 6 ms intervals over three minutes to determine the sensitivity and stability of each detector. Each channel was converted to units of cm^{-1} absorption. To accomplish this, the output of the lock-in amplifier was scaled to account for the lock-in sensitivity and any RF gain after the detector and divided by the total DC output of the detector. This value is then divided by the effective path length, and the product of the Bessel functions. The complete expression is shown in Eq. 6.

Table 1. Technical specifications for the three detector used in this study, including the effective NEP. The noise equivalent power (NEP) for each detector is reported at 10.6 μm, 6 μm, and 730 nm for Det. 1, Det. 2, and Det. 3 respectively.

Detector	Coverage (μm)	NEP (W Hz$^{-1/2}$)	NEP$_{eff}$ (W Hz$^{-1/2}$)	3 dB BW (MHz)
Det. 1	2.5 – 11	4.76×10^{-9}	4.8×10^{-9}	160
Det. 2	2.8 – 6.5	1.67×10^{-12}	6.8×10^{-10}	700
Det. 3	0.35 – 1.1	9.29×10^{-15}	2.2×10^{-13}	2000

Optics EXPRESS

$$\alpha_{cal} = \frac{V_l/(G_l \times G_{RF})}{V_{DC}} \times \frac{1}{L \times (2f/\pi) \times J_0(\beta) \times J_1(\beta)} \quad (6)$$

Here, α_{cal} is the calibrated signal in units of cm^{-1}, V_l is the lock-in amplifier output, G_l is the gain from the lock-in amplifier, G_{RF} is the total gain due to the RF detection electronics, V_{DC} is the DC voltage output of the detector, L is the sample path length, f is the cavity finesse, J_n is the Bessel function of order n, and β is the modulation index. The Allan variance was calculated at binning sizes from 9 times the acquisition time (54 ms) to the total measurement time divided by 9 (20 s) to avoid artifacts that arise from using a small number of bins. The resulting Allan-Werle plots of the most sensitive channel from each detector are shown in Fig. 6 [23].

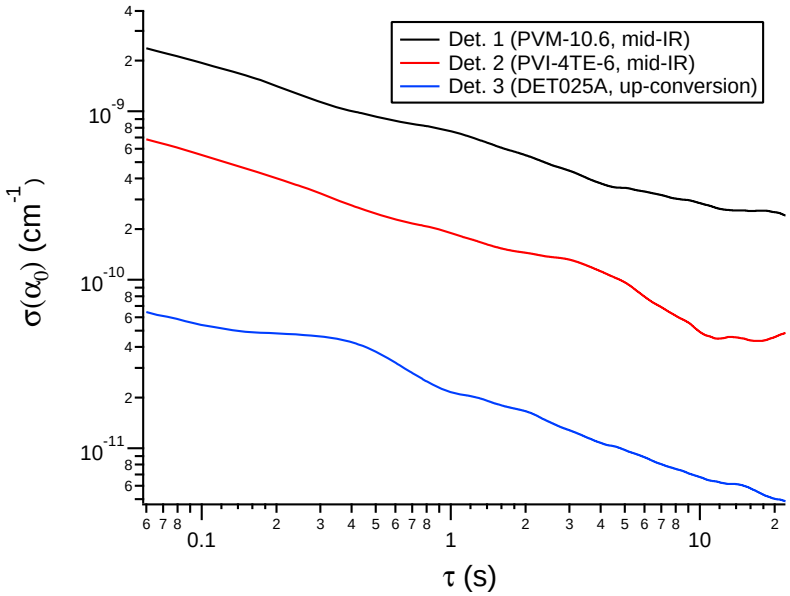

Fig. 6. The Allan deviation of the equivalent absorption as a function of integration time τ. The measurement was taken over 180 s with the H_2 discharge on. The channels shown had the best noise characteristics for each detector.

The Allan deviation for all detectors scaled as $\tau^{-1/2}$, which is characteristic of white noise, up to the maximum integration time of 20 s. The Allan deviation for Det. 1, Det. 2, and Det. 3 with a 2 s time constant were 5.49×10^{-10} cm^{-1}, $1.5\times10^{-10}cm^{-1}$, and $1.7\times10^{-11}cm^{-1}$ respectively. The 3 dB bandwidth for a time constant τ is given by $f_{3dB} = 1/(2\pi\tau)$. This yields an equivalent bandwidth of 0.08 Hz, which gives a NEA of 2.0×10^{-9} cm^{-1} $Hz^{-1/2}$, 5.1×10^{-10} cm^{-1} $Hz^{-1/2}$, and 5.9×10^{-11} cm^{-1} $Hz^{-1/2}$ for Det. 1, Det. 2, and Det. 3 respectively. Therefore, up-conversion was found to be 33 times more sensitive than the original implementation with Det. 1, and is approximately an order of magnitude more sensitive than Det. 2. The improved sensitivity is reflected in the S/N enhancement of a scan of the $R(1,0)$ transition of H_3^+. An example of a scan taken with up-conversion detection using Det. 3 can be seen in Fig. 7. The S/N was channel dependent, and ranged from 2600 - 14600. This is an improvement over the best S/N taken with Det. 1 under the same conditions, which ranged from 1500 to 5700. Although this is a significant improvement over the previous iteration, it does not appear to directly scale with the NEA. There are a few possible explanations for this discrepancy. When the baseline is closely inspected, weak fringes from an etalon still persist which can be seen in Fig. 8. There

Optics EXPRESS

appears to be a short etalon with an FSR of ~1 GHz which is likely arising from the surfaces of the 4 cm PPLN crystal. Also, any connections in the fiber optics after the EOM could give rise to an etalon, which could be responsible for the etalons appearing with a ~30 MHz FSR. These residual etalons are likely limiting the sensitivity when the frequency is scanned.

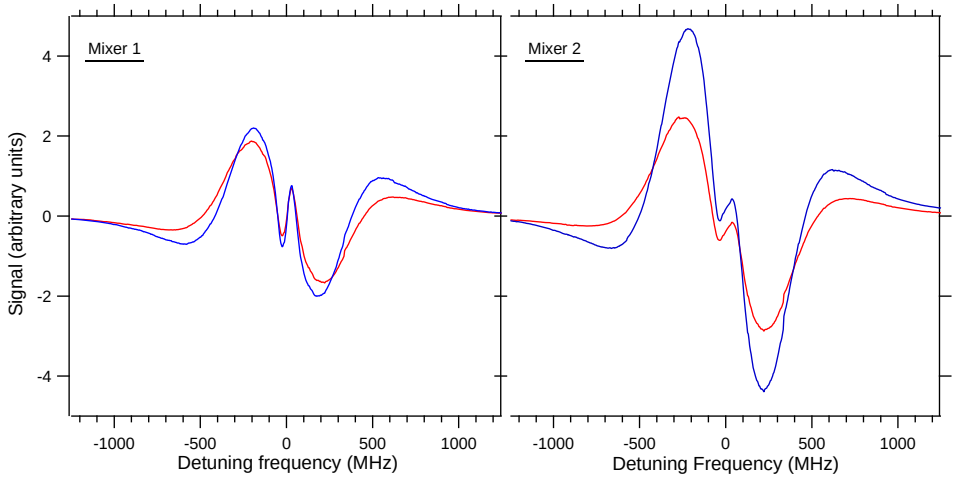

Fig. 7. A NICE-OHVMS scan of the $R(1,0)$ transition of H_3^+ taken with up-conversion detection with Det. 3. The in-phase (red) and quadrature (blue) components of the velocity modulation signal are plotted for both the in-phase (left) and quadrature (right) components of the heterodyne signal. The quadrature component of mixer 2 had a S/N of 14700.

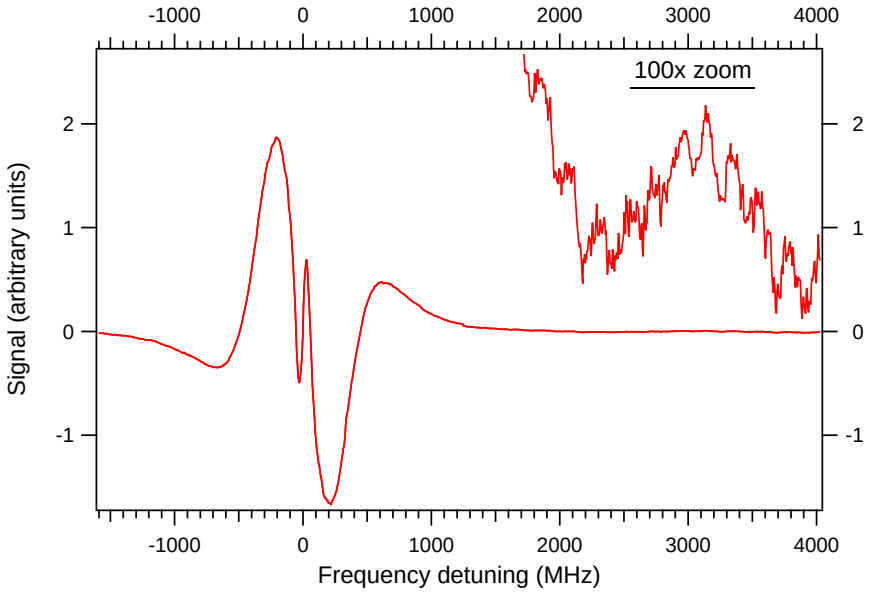

Fig. 8. The in-phase component of mixer 2 of the same scan as Fig. 7, which was observed using up-conversion detection. After scanning past the transition, the sensitivity of the lock-in amplifier was increased to reveal background signals in the baseline.

Optics EXPRESS

The increased bandwidth granted by Det. 2 and up-conversion with Det. 3 also allowed for optimization of the heterodyne modulation frequency. The strength of a NICE-OHMS signal depends on the difference in absorption or dispersion at the sideband and the carrier frequencies and the maximum signal occurs when the modulation frequency is near the full-width at half-maximum (FWHM). Due to limitations with the original detector (Det. 1), we were limited to a modulation frequency of 77 MHz, whereas Doppler broadened transitions of H_3^+ have widths of hundreds of MHz. Detector 2 and 3 have the necessary bandwidth to operate with optimized heterodyne frequencies near the FWHM.

A comparison between scans collected with a heterdoyne frequency of 1, 3, and 5×FSR of the cavity using Det. 2 can be seen in Fig. 9. To compare the signal strength between scans at different detection angles, it is useful to compare the peak-to-peak signal strength summed in quadrature. The total signal was found to be optimized at 3×FSR of the cavity at 231 MHz, which was stronger by a factor of 3.6 in comparison to the 1×FSR scans.

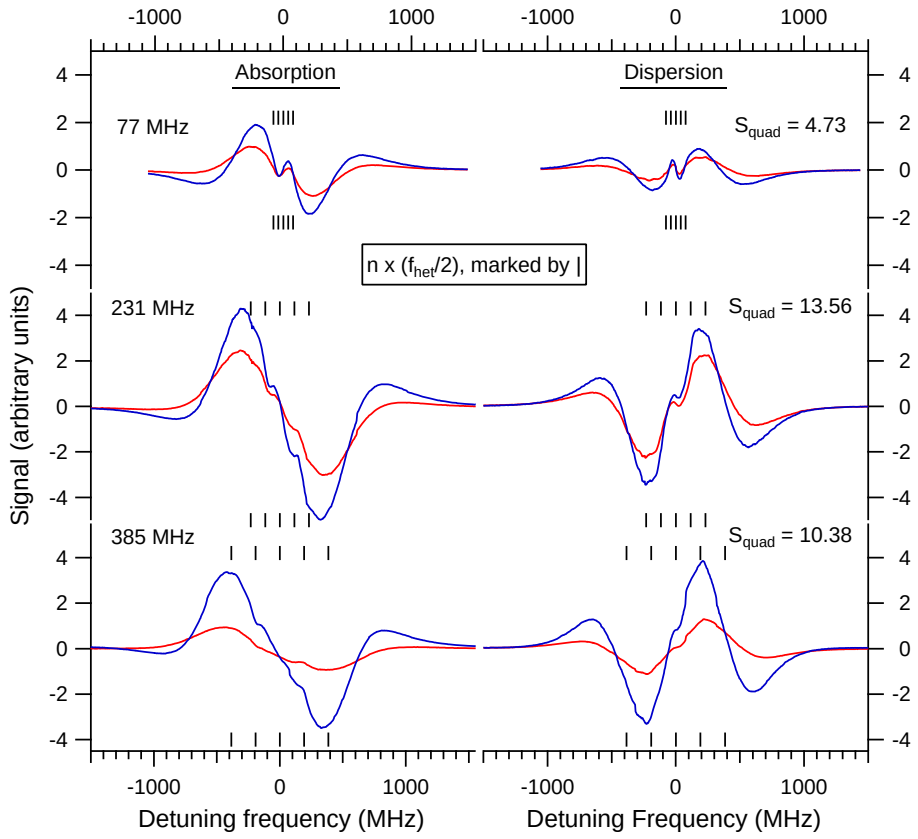

Fig. 9. A comparison between scans taken with the heterodyne frequency set to 1, 3, and 5×FSR of the cavity with Det. 2. The in-phase component of velocity modulation is shown in red and the quadrature component in blue. The output of the mixers were set for absorption and dispersion shown on the left and right respectively. The vertical dashes are centered at the rest frequency and separated in half-integer multiples of the heterodyne frequency to indicate the expected Lamb dip frequencies. The peak-to-peak signal of all four channels summed in quadrature is denoted as S_{quad}.

Scans with higher heterodyne frequencies were able to resolve the individual Lamb dips,

Optics EXPRESS

which were found to have a width of approximately 70 MHz. This can be clearly seen in Fig. 9 in the absorption channels where the Lamb dips overlap when the heterodyne frequency was 77 MHz and become resolved at 231 and 385 MHz. Unfortunately, the Lamb dips appeared to become smaller as the heterodyne frequency increased. It is possible that the heterodyne frequency was not perfectly matched to a multiple of the cavity's FSR, which would result in a weaker Lamb dip. This could be avoided in future experiments by locking the sidebands onto resonance with DeVoe-Brewer locking [24].

Despite the smaller sub-Doppler features, resolving the individual Lamb dips opens doors to new experiments that were impossible with overlapping features. The narrower sub-Doppler feature could allow for resolving hyperfine structure. In a recent NICE-OHVMS study of OH^+, transitions with hyperfine components separated by ~120 MHz were treated as intensity-weighted averages [10]. A narrower central Lamb dip would enable resolved structure which would improve the predictions of the pure rotational spectra.

4. Conclusion

This work demonstrates that up-conversion detection and Brewster-plate spoilers are viable options for improving the sensitivity of the NICE-OHVMS technique in the mid-IR, and could be used in other NICE-OHMS instruments. When up-conversion was used with a Si biased detector, the NEA was improved by two orders of magnitude in comparison to the previous mid-IR detector. Additionally, to our knowledge this study is the first demonstration of a Brewster-plate spoiler in a cavity enhanced experiment, which effectively averaged out parasitic etalons in our measurements. Together, up-conversion detection and the Brewster-plate spoilers will enable precise measurements of transitions which were previously too weak to observe. We plan to use the improvements to complete the high-precision survey of H_3^+ transitions and explore new targets that were previously undetectable.

Funding

National Aeronautics and Space Administration (NASA) (NNX13AE62G, NNX16AO86H); National Science foundation (NSF) (PHY 14-04330, CHE 12-13811)

Acknowledgments

C.R.M. is grateful for support from a NASA Earth and Space Science Fellowship (NESSF NNX16AO86H). We would like to thank Jefferson McCollum, Phillip Kocheril, and Thomas Dieter for their assistance in aligning the difference frequency generation optics.